

# High performance CO<sub>2</sub> Absorption/Desorption using Amine-Functionalized magnetic nanoparticles

Fariba Zarei, Peyman Keshavarz\*

School of Chemical and Petroleum Engineering, Shiraz University, Shiraz, Iran



## ARTICLE INFO

**Keywords:**  
Carbon Dioxide  
Absorption  
Desorption  
Fe<sub>3</sub>O<sub>4</sub>  
Functionalized  
Nanoparticles

## ABSTRACT

In the current study, for the first time, a variety of amino acid groups, including arginine, histidine, and glycine, were added to Fe<sub>3</sub>O<sub>4</sub> nanoparticles to achieve desired mass and heat transfer properties in CO<sub>2</sub> absorption/desorption experiments. For this purpose, different concentrations of synthesized nanoparticles were employed in base fluid (10 wt% methyl diethanolamine) in a semi batch experiment at ambient pressure for CO<sub>2</sub> absorption and desorption. The experimental results clearly indicated that modification of iron oxide nanoparticles could enhance CO<sub>2</sub> absorption and stripping significantly, as a result of higher stability of nanoparticles and presence of amino groups at the nanoparticles' structure. Compared to bare Fe<sub>3</sub>O<sub>4</sub>, Fe<sub>3</sub>O<sub>4</sub>@arginine, Fe<sub>3</sub>O<sub>4</sub>@histidine, and Fe<sub>3</sub>O<sub>4</sub>@glycine demonstrated 23%, 17%, and 10% increase in CO<sub>2</sub> absorption capacity, respectively. By using chemical agent as stabilizer species and by modified thermal properties of solution, magnetic nanoparticles promoted CO<sub>2</sub> desorption to a great extent. Therefore, Fe<sub>3</sub>O<sub>4</sub>@arginine, Fe<sub>3</sub>O<sub>4</sub>@histidine, and Fe<sub>3</sub>O<sub>4</sub>@glycine nanofluids improved CO<sub>2</sub> desorption enhancement by 48.2%, 47.2%, and 46.1% at 70 °C, respectively.

## 1. Introduction

As a result of human activity, the average atmospheric temperature has recently been increasing, posing a serious environmental threat [1]. Thus, numerous researchers have done studies to cut greenhouse gas emissions and their negative effects, such as acidic rain and snow. Consequently, these studies demonstrated that carbon dioxide intensified global warming to a great extent [2]. Offering practical methods for CO<sub>2</sub> capture have therefore been known as effective strategies for reducing climate change. The CO<sub>2</sub> capture methods were classified into three basic categories: pre-combustion, oxy-fuel combustion, and post-combustion [3–5]. Among these methods, it was post-combustion CO<sub>2</sub> capture which received considerable attention because of its advantages, such as high performance for CO<sub>2</sub> separation and low CO<sub>2</sub> partial pressure in gas stream [6,7]. In addition, it included several effective methods such as low-temperature distillation, membranes, and physical and chemical adsorption [8–10]. Among the methods embedded into post-combustion, CO<sub>2</sub> absorption by physical and chemical absorbents was a common industrial method [11]. Between them, amine solutions were attracted considerable attention by numerous researcher [12]. However, high energy requirements at solvent regeneration sections posed a serious challenge for CO<sub>2</sub> absorption. Therefore, in order to

reduce regeneration energy consumption, the scientists conducted a number of studies and found that adding acidic catalysts [13–18] or applying ultrasonic [19–23] or microwaves [24–29] during the regeneration process were among the effective methods for reducing regeneration energy consumption. In addition, blend amines was recognized as a favorable method in enhancing CO<sub>2</sub> absorption and desorption performance, that was investigated theoretically and empirically [30]. However, applying nanoparticles was known as the best choice than the mentioned methods due to their high efficiency in absorption and stripping CO<sub>2</sub>. Since nanoparticles had different mechanisms, they performed better in terms of CO<sub>2</sub> absorption/desorption. Regarding CO<sub>2</sub> absorption, several mechanisms, such as hydrodynamic effect, shuttle effect, and Brownian motion, contributed to increasing nanofluids' ability to absorb CO<sub>2</sub> [31,32]. However, nanoparticles' thermal properties along with hydrodynamic effect significantly enhanced CO<sub>2</sub> stripping. Accordingly, several studies were conducted for the purpose of investigating nanoparticles' thermal properties. A study carried out by Chio and Eastman (1995) revealed that adding nanoparticles could increase the thermal conductivity of base fluid by 40% [33]. Furthermore, Kebinski et al., (2002) investigated a number of effective mechanisms, including liquid layering, NP clustering, and Brownian motion, to enhance the thermal conductivity [34]. In addition, Prasher et al.,

\* Corresponding author.

E-mail address: [pkeshavarz@shirazu.ac.ir](mailto:pkeshavarz@shirazu.ac.ir) (P. Keshavarz).

(2006) explored the impact of Brownian motion on improvement of the thermal conductivity [35]. As a result of these studies, nanoparticles were found to be effective in intensifying CO<sub>2</sub> stripping. Thus, to investigate the effectiveness of nanoparticles on CO<sub>2</sub> desorption, several studies summarized in Table 1 were conducted.

The high performance of Fe<sub>3</sub>O<sub>4</sub> nanoparticles on rising CO<sub>2</sub> uptake and stripping was demonstrated in the literature study [42]. It is noticeable that magnetic nanoparticles have many different advantages including superparamagnetic properties, high surface-to-volume ratio, low toxicity, reutilization and effective recovery [44,45]. However, good thermal properties of magnetic nanoparticles are not insignificant in improving heat transfer process. Nonetheless, they have very low stability in the base fluid at high concentration, and it is considered as the main challenge in using magnetic nanoparticles in the mass transfer processes. However, numerous researchers demonstrated that adding amines to nanoparticles' surfaces can be an efficient strategy to improve nanoparticles hydrophilic properties. On the other hand, amines can be effective in increasing CO<sub>2</sub> absorption by chemical and physical mechanisms. Accordingly, numerous studies investigated the positive effect of functionalized nanoparticles in enhancing CO<sub>2</sub> capture [46–48]. Nonetheless, to the best of researcher's knowledge, the influence of functionalized nanoparticles on enhancing solvent regeneration rates was not examined. In other words, there are no available experimental or theoretical studies on CO<sub>2</sub> absorption/desorption using functionalized Fe<sub>3</sub>O<sub>4</sub> nanoparticles. Hence, several functionalized magnetic nanoparticles were used in this study for both absorption and desorption of CO<sub>2</sub>. The key point in our work is that this is the first study of employing functionalized nanoparticles in improving CO<sub>2</sub> desorption performance. Indeed, in this work, the regeneration process was investigated at low temperatures to examine the real power of nanoparticles in intensified CO<sub>2</sub> stripping. Thus, the amino acids of arginine, histidine, and glycine were applied to the surface of Fe<sub>3</sub>O<sub>4</sub> nanoparticles. Subsequently, the amount of CO<sub>2</sub> at the outlet gas and liquid phases was analyzed, and the effect of temperature, nanoparticles type, and concentration on CO<sub>2</sub> stripping enhancement was investigated.

## 2. Experimental methods

### 2.1. Preparation of nanoparticles

#### 2.1.1. Preparation of Fe<sub>3</sub>O<sub>4</sub> nanoparticles

The Fe<sub>3</sub>O<sub>4</sub> nanoparticles was prepared by the co-precipitation method. As can be seen in Fig. 1, in the first step, a mixture of 4.8 mmol of FeCl<sub>3</sub>·6H<sub>2</sub>O, 4.5 mmol of FeCl<sub>2</sub>·4H<sub>2</sub>O, and 1 g of polyvinyl alcohol (PVA 15000) was added to 30 mL deionized water. Then, the mechanical stirrer and heater stirrer were used for homogenization of the solution; after this, the solution was heated to 80 °C, until the mixture turned a brown color. At this time, the 10 v/v% ammonium hydroxide solution was added slowly to reach pH 10 and a dark precipitate was observed. Subsequently, magnetic field was employed to separate the formed precipitate from the mixture.

Finally, the precipitates were washed three times with deionized water and ethanol and then were dried in vacuum oven at 80 °C for 12 h.

#### 2.1.2. Preparation of functionalized nanoparticles

To prepare Fe<sub>3</sub>O<sub>4</sub>@gly, Fe<sub>3</sub>O<sub>4</sub>@his and Fe<sub>3</sub>O<sub>4</sub>@arg nanoparticles, synthesized Fe<sub>3</sub>O<sub>4</sub> nanoparticles was employed. In this regard, a homogeneous solution of 300 mL deionized water and mixture of 10.8 mmol Fe<sub>3</sub>O<sub>4</sub> nanoparticles and 7.5 mmol from each of the amino acids (glycine, histidine and arginine) was prepared. Next, the mechanical stirrer and heater were used for 2 h at 80 °C. Finally, the formed precipitates were collected, washed (three times with deionized water and ethanol) and dried (at 50 °C for 24 h).

**Table 1**  
Summary of other researchers' studies on CO<sub>2</sub> desorption by nanofluids.

Authors	Base fluid	Nanoparticles	Conclusion	Ref
Lee et al.	Distilled water	SiO <sub>2</sub> , Al <sub>2</sub> O <sub>3</sub>	SiO <sub>2</sub> nanoparticles was efficient in improving CO <sub>2</sub> uptake and regeneration up to 23.5% and 11.8 %, respectively. CO <sub>2</sub> absorption was improved to 23.5% by Al <sub>2</sub> O <sub>3</sub> nanofluids, but the desorption performance was reduced by about 11.2%	[36]
Yu et al.	30 wt% MDEA 30 wt% MEA 1.5 mol/L PZ	TiO <sub>2</sub> , SiO <sub>2</sub> , CuO and Al <sub>2</sub> O <sub>3</sub>	The regeneration performance was improved by adding TiO <sub>2</sub> following CuO, SiO <sub>2</sub> and Al <sub>2</sub> O <sub>3</sub> , respectively.	[37]
Lee et al.	Methanol	SiO <sub>2</sub> , Al <sub>2</sub> O <sub>3</sub>	The effect of nanoparticles on several properties of heating surface, including density of nucleation sites, roughness, wettability and bubble detachment time were investigated. Al <sub>2</sub> O <sub>3</sub> nanoparticles could enhance CO <sub>2</sub> uptake efficiency up to 16% compared to base fluid (pure methanol).	[38]
Wang et al.	30 wt% MEA	SiO <sub>2</sub> , TiO <sub>2</sub> , Al <sub>2</sub> O <sub>3</sub>	nano particles result in increased CO <sub>2</sub> absorption rate of over 10% Time of Desorption process can be reduced by 42% in presence TiO <sub>2</sub> nanoparticles at 0.1 wt% concentration.	[39]
Shakir et al.	MEA + TEA	SiO <sub>2</sub> , Al <sub>2</sub> O <sub>3</sub> and Fe <sub>2</sub> O <sub>3</sub>	Compared to base fluid, the CO <sub>2</sub> absorption was increased by 28%, 19% and 15% using the Al <sub>2</sub> O <sub>3</sub> , Fe <sub>2</sub> O <sub>3</sub> and SiO <sub>2</sub> nanoparticles at optimum concentration.	[40]
Hafizi et al.	water	Functionalized-Fe <sub>3</sub> O <sub>4</sub>	Fe <sub>2</sub> O <sub>3</sub> , SiO <sub>2</sub> , and Al <sub>2</sub> O <sub>3</sub> nanofluids enhanced the CO <sub>2</sub> desorption rate to 47%, 28%, and 22%, respectively. The absorption capacity was improved 77 % using functionalized magnetic nano-fluid at 293.15 K. The regeneration energy was reduced about 23.2 % by employing sonicated-based regeneration procedure. The higher CO <sub>2</sub> solubility, lower reduction in cyclic absorption/desorption capacity and higher energy efficiency of CO <sub>2</sub> absorption/desorption process were achieved using the functionalized-magnetic nanoparticles and sonication-based regeneration procedure.	[41]
Zarei et al.	10 wt% MDEA	SiO <sub>2</sub> , TiO <sub>2</sub> , CuO and Fe <sub>3</sub> O <sub>4</sub>	Fe <sub>3</sub> O <sub>4</sub> nanoparticles had highest impact in improving CO <sub>2</sub> absorption. 0.01 wt% Fe <sub>3</sub> O <sub>4</sub> enhanced	[42]

(continued on next page)

**Table 1 (continued)**

Authors	Base fluid	Nanoparticles	Conclusion	Ref
Li et al.	DBU-glycerol	SiO <sub>2</sub>	<p>the CO<sub>2</sub> loading up to 36%.</p> <p>metal oxide nanoparticles were more efficient in intensified CO<sub>2</sub> desorption</p> <p>0.05 wt% CuO nanoparticles increased CO<sub>2</sub> concentration at outlet gas phase up to 44.2 vol% at 70 °C regeneration temperature.</p> <p>The average particle size was reduced by enhancing proper ultrasonic vibration time and nanoparticles loading, which lead to improve the absorption performance.</p> <p>For small SiO<sub>2</sub> nanoparticles (size is 102 nm or below) gas-liquid interfacial area had little effect on the enhancement factor.</p> <p>Compared to the base fluid, the absorption rate was just up to 31 % using 0.10 wt% SiO<sub>2</sub> nanoparticle with particle size of 16 nm.</p> <p>In regeneration process, the desorption rate of nano fluid was increased 18 % using 0.10 wt% nanoparticle (particle size of 32 nm).</p> <p>Nanoparticles was recognized as a good candidate to improve CO<sub>2</sub> absorption and desorption performance.</p>	[43]

## 2.2. Nanofluid preparation

In this study, all nanoparticles were prepared as in the above procedure, as follows: 10 wt% solution of methyl diethanolamine (MDEA) was employed as base fluid in 1700 mL. Next, the nanofluid was

prepared by adding different weight of synthesized Fe<sub>3</sub>O<sub>4</sub>, Fe<sub>3</sub>O<sub>4</sub>@arg, Fe<sub>3</sub>O<sub>4</sub>@his, Fe<sub>3</sub>O<sub>4</sub>@gly nanoparticles. So, 0.170, 0.513 and 0.851 g from each of the nanoparticles were used to achieve nanofluid with 0.01 wt%, 0.03 wt% and 0.05 wt% nanoparticles concentrations, respectively. To prevent sedimentation of nanoparticles in base fluid, ultrasonic irradiation (Tomy, UD-201, Japan) was applied on nanofluid for 30 min. In addition, for all nanofluids, C-Tab surfactant with 1:1 wt ratio (nanoparticles to surfactant) was used to prevent nanoparticles agglomeration.

## 2.3. Experimental setup

In this work, CO<sub>2</sub> absorption/desorption tests were performed using a bubble column contactor at ambient pressure that is shown in Fig. 2. This semi-batch contactor is made with a plexiglass column having a 3000 mL effective volume as the main part of this apparatus. In addition, to introduce a bubble-shaped inlet gas stream in the column, an air stone was installed on the bottom section of the column. To use described experimental setup for both absorption/desorption experiments, an electrical heating element (with 3–5 min delay time to achieve the desired temperature) and temperature controller system (a thermostat with 0.1 °C precision) were located in the center of the column. So, the required temperature in regeneration part was provided and fixed at desired set point during the regeneration process. Moreover, to analyze the nanofluids, a tube sampler was installed at the bottom platform of the device. In addition, to analysis of outlet gas phase, first, the moisture in the outlet gas stream was removed using a silica gel column, and then a gas flow meter and CO<sub>2</sub> analyzer were installed to record outlet gas flow rate and its CO<sub>2</sub> volume fraction, that were placed on the top of the column.

## 2.4. Experimental procedure

In the first section, the CO<sub>2</sub> absorption tests were done at atmospheric pressure and 20 °C in described semi batch device. At this point, 1700 mL of prepared desired nanofluid was poured into column and pure CO<sub>2</sub> (purity >99%) at constant flow rate (175 mL/min) was injected to nano-solvent as bubble shapes for 45 min. It is noticeable that the CO<sub>2</sub> loading in liquid phase (mole of CO<sub>2</sub> to mole of amine) was employed to express CO<sub>2</sub> absorption and desorption performance. For this purpose, the CO<sub>2</sub> content in nano solution was determined using precipitate method. Thus, 20 mL liquid sample was assembled at 10, 20, 30 and 45 min of each absorption experiment to determine CO<sub>2</sub> loading

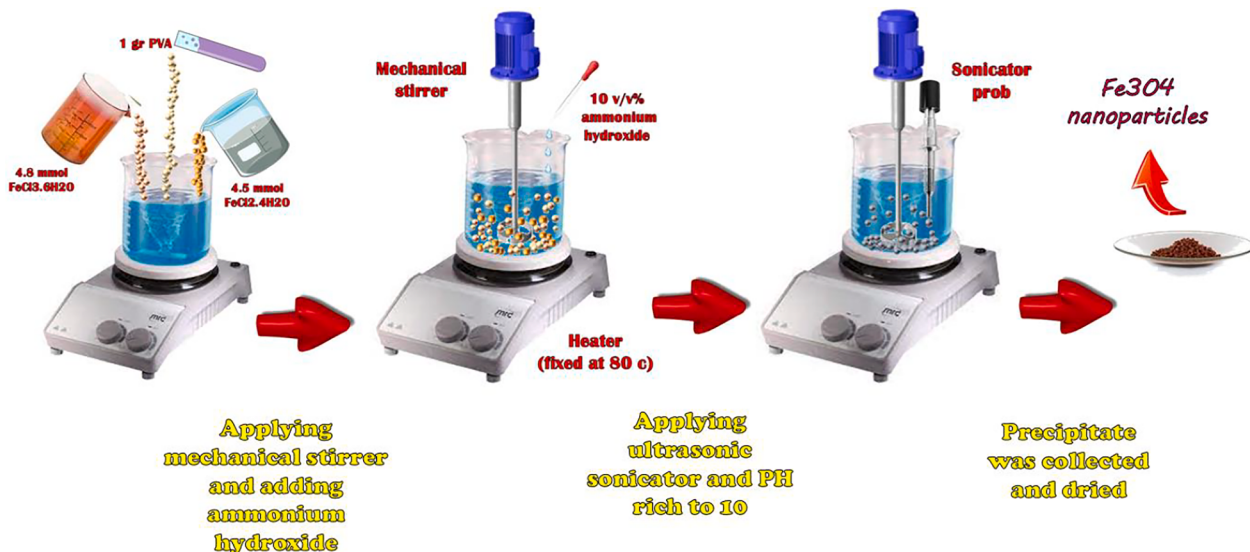


Fig. 1. Process of synthesis Fe<sub>3</sub>O<sub>4</sub> nanoparticles.

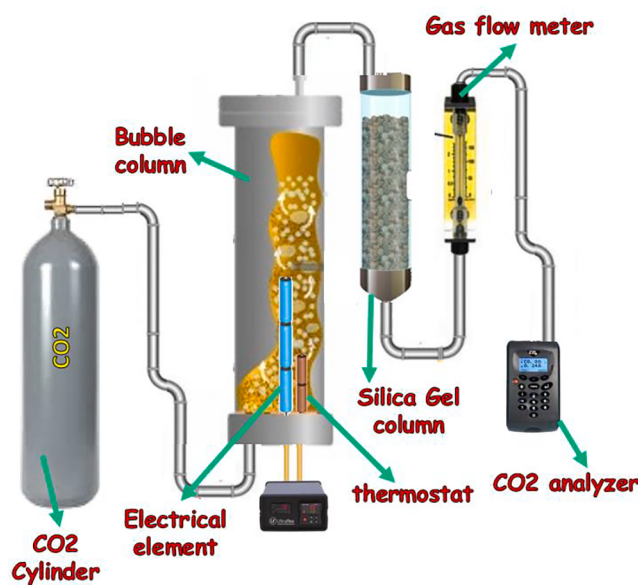


Fig. 2. Schematic diagram of the experimental setup.

in liquid phase. Next, at the end of absorption experiment, the solvent regeneration was done for 72 min. Thus, nanofluid heating was started using thermal coil at fixed set point temperatures (60 and 70 °C). In addition, the purge air with 200 mL/min flow rate was applied to column by air stone, during the regeneration time. In these tests, to investigate the CO<sub>2</sub> stripping performance from the nanofluid, the outlet gas flow rate and its CO<sub>2</sub> concentration were recorded every 3 min. At the end of regeneration experiments, another liquid sample was collected. To determine the CO<sub>2</sub> loading of liquid phase by precipitate method [49], 1 M NaOH solution was added in excess to liquid sample to convert CO<sub>2</sub> molecules to nonvolatile component. Next, 1 M BaCl<sub>2</sub>·2H<sub>2</sub>O solution was added in excess as previous step and the sample was stirred to create stable BaCO<sub>3</sub> precipitate. Then, the precipitate was filtered, dried and weighted. Finally, the following correlations were employed to determine the CO<sub>2</sub> loading as CO<sub>2</sub> mole per mole of amine solution, based on the weight of BaCO<sub>3</sub> precipitate:

$$n_{CO_2} = \frac{m_{pre}}{MW_{BaCO_3}} \quad (1)$$

$$w_{amine} = w_{sample} \times C \quad (2)$$

$$n_{amine} = \frac{w_{amine}}{MW_{amine}} \quad (3)$$

$$CO_2 loading = \frac{n_{CO_2}}{n_{amine}} \quad (4)$$

where  $m_{pre}$ ,  $MW_{BaCO_3}$ ,  $w_{sample}$ ,  $C$  and  $MW_{amine}$  are defined as mass of precipitate as g, BaCO<sub>3</sub> molecular weight, weight of sample, amine solution concentration and amine molecular weight, respectively.

All the experiments were repeated three times to avoid uncertainty in the experimental results.

### 3. Nanoparticles characterization

#### 3.1. X-Ray diffraction analysis (xrd)

To investigate the synthesized iron oxide nanoparticles, X-ray diffraction characterization was utilized, and the reference pattern (JCPDS number 01-079-0417) was compared with XRD patterns for Fe<sub>3</sub>O<sub>4</sub> nanoparticles. As it is clear from Fig. 3, the peaks at  $2\theta = 30.1$ , 35.4, 43.1, 53.4, 57 and 62.6° reflect Fe<sub>3</sub>O<sub>4</sub> crystal planes. Furthermore,

the low inert peak confirms the high purity of all synthesized nanoparticles.

#### 3.2. Scanning electron microscope (sem) and transmission electron microscopy (tem) analysis

The structure, size, and morphology of synthesized nanoparticles were examined using Scanning Electron Microscope (SEM, TESCAN-Vega 3, Czech Republic) and Transmission Electron Microscopy (TEM, Philips EM 208S) was used. As shown in Fig. 4 and Fig. 5, all Fe<sub>3</sub>O<sub>4</sub>@gly, Fe<sub>3</sub>O<sub>4</sub>@his and Fe<sub>3</sub>O<sub>4</sub>@arg, was 8–12 nm, 12–17 nm, 15–21 nm and 18–24 nm, respectively. Therefore, Fe<sub>3</sub>O<sub>4</sub> was functionalized properly, and all functionalized nanoparticles were larger than Fe<sub>3</sub>O<sub>4</sub> nanoparticles. Table 2 summarizes the results of nanoparticles characterization.

#### 3.3. Fourier transform infrared spectroscopy analysis

FTIR analysis was used to explore the molecular bonds of synthesized magnetic nanoparticles. Fe<sub>3</sub>O<sub>4</sub>, Fe<sub>3</sub>O<sub>4</sub>@arg, Fe<sub>3</sub>O<sub>4</sub>@his and Fe<sub>3</sub>O<sub>4</sub>@gly spectra were measured by Bruker spectrophotometer (model Tensor II, accuracy of 5%, Germany). Based on FTIR results indicated in Fig. 6, the peak between 540–560 cm<sup>-1</sup> was attributed to Fe–O bond. Moreover, the presence of amino groups in the structure of functionalized nanoparticles led to the observation of vibrations around 3100 and 3400 cm<sup>-1</sup> corresponded to O–H and N–H bonds, respectively. Thus, FTIR analysis showed that amino acids were successfully applied to Fe<sub>3</sub>O<sub>4</sub> nanoparticles surface.

#### 3.4. Thermo gravimetric analysis (tga)

The thermal properties of bare and functionalized Fe<sub>3</sub>O<sub>4</sub> were explored using TGA analysis. As shown in Fig. 7, TGA tests were conducted at 25–800 °C with a 10C/min heating ramp under nitrogen flow as purge gas. Furthermore, it is evident in this table that the first weight loss occurred at about 200 °C, which was attributed to this moisture removal from samples. It was found that all functionalized Fe<sub>3</sub>O<sub>4</sub> decomposed at about 300 °C. As a result, at 60 and 70 °C temperatures, nanoparticles' degradation and decomposition were very low in regeneration process.

### 4. Results and discussion

#### 4.1. Mass and heat transfer mechanisms in nanofluids

In previous studies, the various effective mechanisms in mass and heat transfer processes in nanofluids have been discussed including Brownian motion, bubble breaking, macro-convection, shuttle effect, and thermal conductivity effect, [50–52].

According to the studies reviewed in the literature, Brownian motion

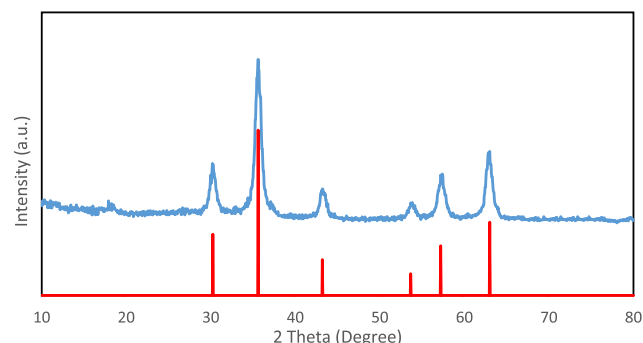


Fig. 3. XRD patterns of Fe<sub>3</sub>O<sub>4</sub> nanoparticles.

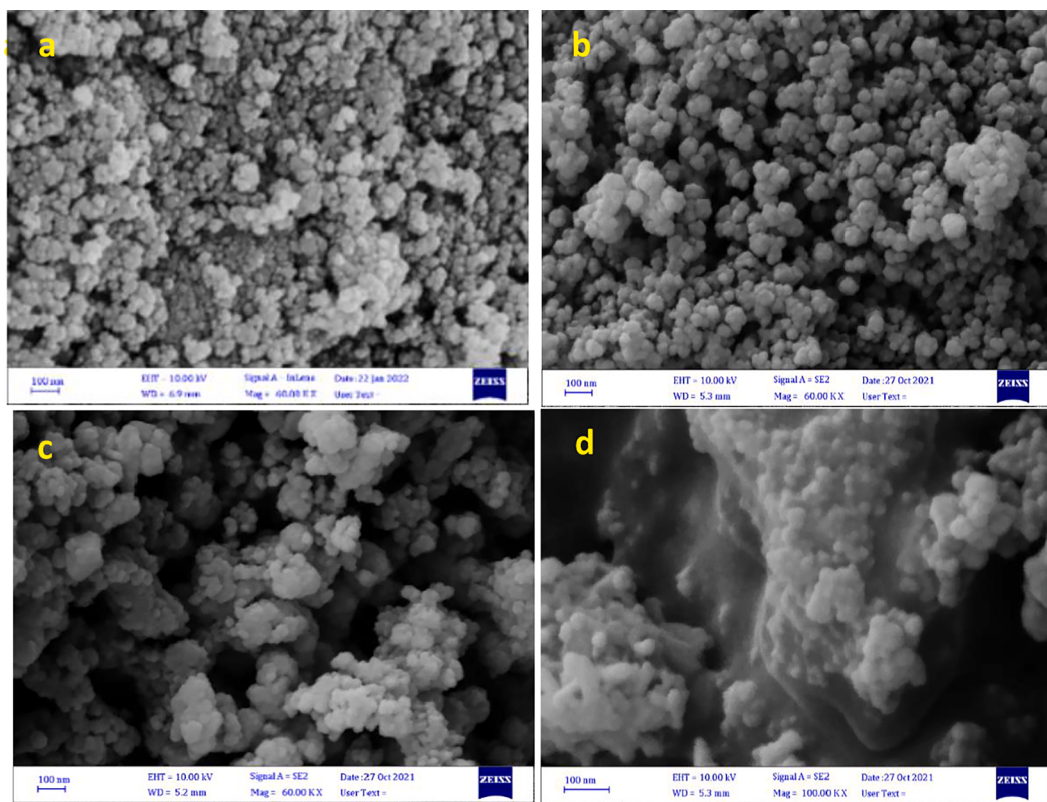


Fig. 4. The FE-SEM analysis result for a)  $\text{Fe}_3\text{O}_4$ , b)  $\text{Fe}_3\text{O}_4@\text{gly}$ , c)  $\text{Fe}_3\text{O}_4@\text{his}$  and d)  $\text{Fe}_3\text{O}_4@\text{arg}$ .

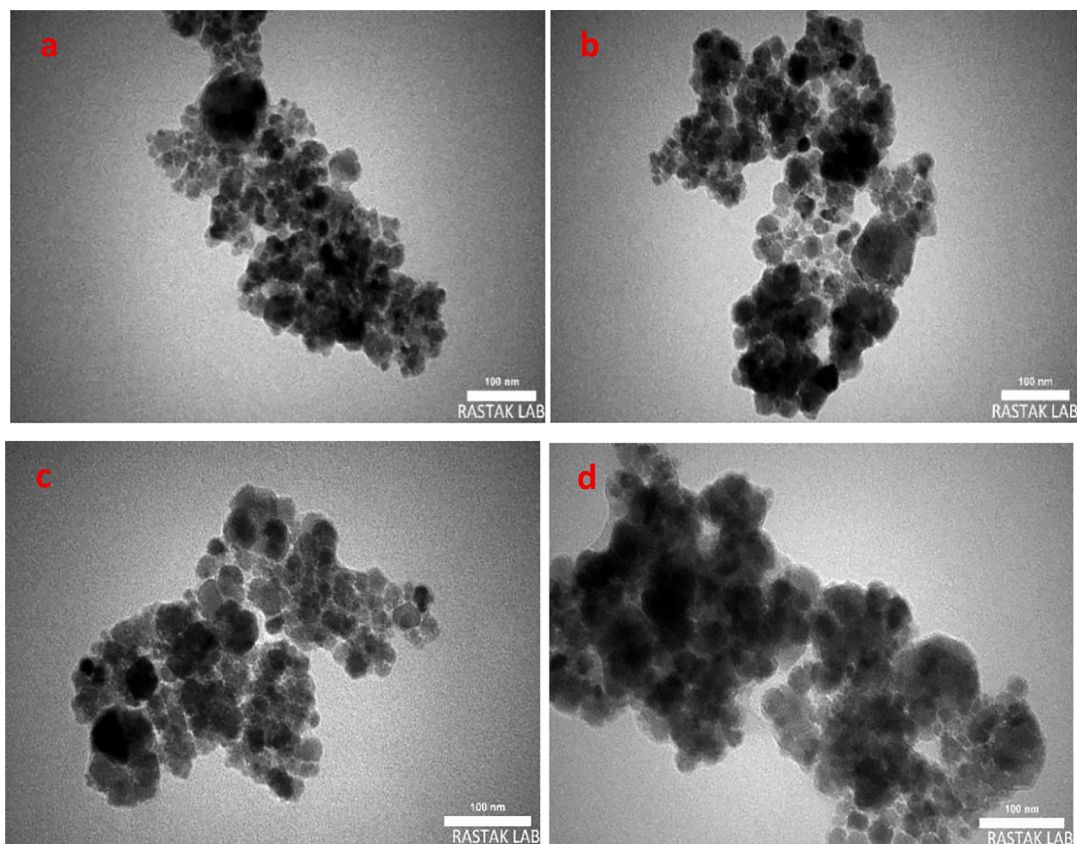


Fig. 5. The TEM analysis result for a)  $\text{Fe}_3\text{O}_4$ , b)  $\text{Fe}_3\text{O}_4@\text{gly}$ , c)  $\text{Fe}_3\text{O}_4@\text{his}$  and d)  $\text{Fe}_3\text{O}_4@\text{arg}$ .

**Table 2**  
Nanoparticles characterization.

Name	Color	Morphology	Average particle size (nm)
Fe <sub>3</sub> O <sub>4</sub>	Dark brown	Spherical	8–12
Fe <sub>3</sub> O <sub>4</sub> @gly	Dark brown	Spherical	12–17
Fe <sub>3</sub> O <sub>4</sub> @his	Dark brown	Spherical	14–18
Fe <sub>3</sub> O <sub>4</sub> @arg	Dark brown	Spherical	15–22

as one of the most crucial mechanisms can improve significantly the rate of mass and heat transfer in nanofluids. Since the added particles possess more kinetic energy, the addition of nanoparticles to a base fluid can intensify the Brownian motion of micro-molecules in the fluid. Therefore, in nanofluids, the components were distributed faster compared to the conventional fluids. In addition, energy transfer in nanofluids was facilitated by collisions between nanoparticles with high thermal conductivity and solvent molecules. Thus, it can be concluded that the use of nanoparticles as an active agent with high kinetic energy can establish a better heat and mass transfer in the base fluid [53,54].

In gas–liquid systems such as bubble columns or tray towers, dynamic nanoparticle collisions with gas bubbles can cause to break down them into smaller bubbles, resulting in an increased effective interfacial area between the gas and liquid phases and also it can increase the turbulence of system [50,55].

On the other hand, the movement of nanoparticles resulted in significant micro convection within the base fluid. Therefore, it enhances the local turbulence in liquid phase, refreshing the gas–liquid boundary layer, and reducing the mass transfer resistance of the liquid phase [56,57].

It has been observed that the presence of nanoparticles can lead to an increase in absorption capacity, and the mechanism responsible for this enhancement is known as the shuttle effect. Various studies have highlighted that some molecules in nanofluids tend to adsorb on the surface of nanoparticles at the gas–liquid interface and are transported to deeper layers of the liquid. This effect facilitates a better diffusion of solute to the solvent media. Furthermore, the adsorption on the surface of nanoparticles can enhance the gas absorption capacity of the base fluid [58,59].

Based on these mechanisms, nanoparticles having smaller particle size and greater stability exhibit a greater impact on enhancing mass and heat transfer. In other words, suspended particles with higher stability

can produce higher hydrodynamic effects, greater available surface area, and more turbulence within the liquid phase [60–62].

Applying nanoparticles is known to enhance thermal conductivity, making it an essential factor in improving rate of heat transfer. Multiple theoretical and empirical studies have demonstrated that the thermal conductivity of a base fluid can be enhanced by the presence of nanoparticles. Specifically, adding nanoparticles with a higher thermal conductivity than the base fluid can increase the average thermal conductivity of the resulting nanofluid. Thus, this improvement in thermal conductivity can intensify the heat diffusivity within the nanofluid and lead to a more efficient heat transfer process. It is noticeable that this phenomena has been subject to various explanations, including molecular-level layering, Brownian motion, and the nature of nanoparticles and base fluid which were discussed in the previous research [34,63].

#### 4.2. Stability of nanoparticles

Numerous studies have utilized zeta potential analysis to determine the stability of nanoparticles in the base fluid [64–67]. As a result, the stability of nanofluids was evaluated using zeta potential analysis in this study (Horiba SZ-100 DLS, central laboratory of Shiraz University).

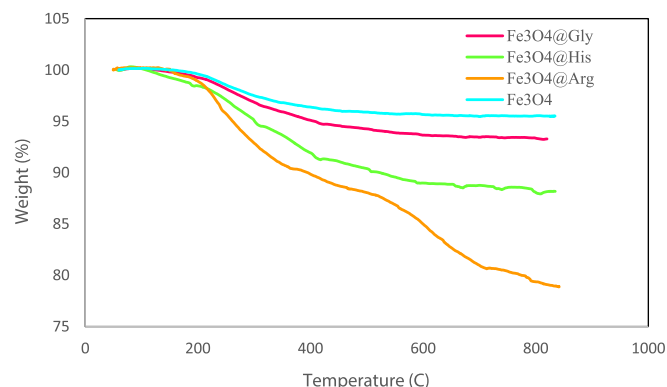


**Fig. 7.** TGA graph of the Fe<sub>3</sub>O<sub>4</sub>, Fe<sub>3</sub>O<sub>4</sub>@gly, Fe<sub>3</sub>O<sub>4</sub>@his and Fe<sub>3</sub>O<sub>4</sub>@arg nanoparticles.

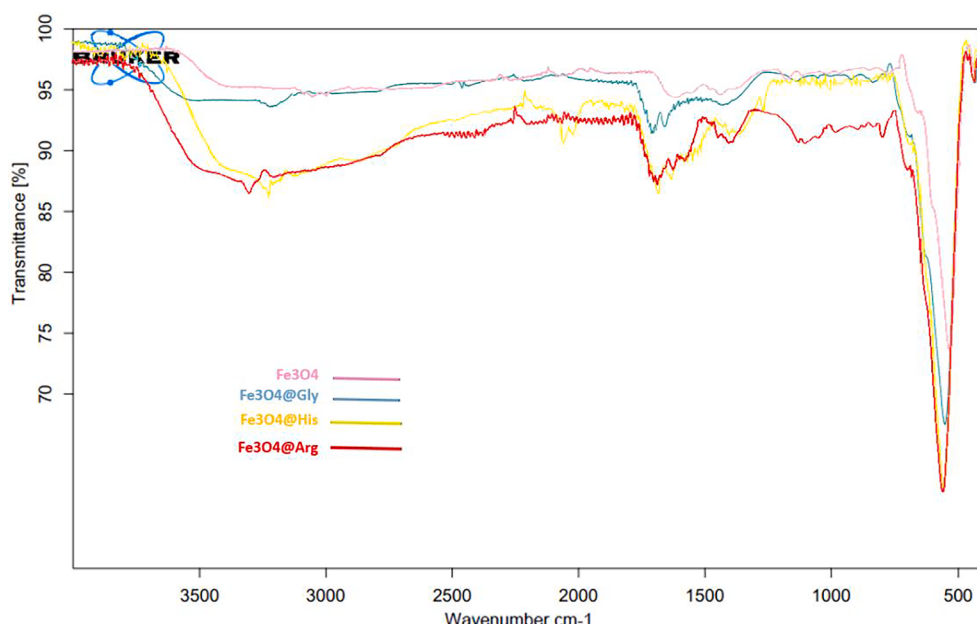


**Fig. 6.** FTIR spectra for Fe<sub>3</sub>O<sub>4</sub>, Fe<sub>3</sub>O<sub>4</sub>@gly, Fe<sub>3</sub>O<sub>4</sub>@his and Fe<sub>3</sub>O<sub>4</sub>@arg nanoparticles.

Absolute zeta potential values generally confirmed the stability, low stability or instability of nanofluids. Hence, the stable nanofluids had absolute zeta potential in the range of 30–60 mV. In addition, nanofluids with 20–30 mV absolute zeta potential had low stability, and were not stable at lower values of absolute zeta potential. Hence, the stability of all nanofluids investigated was summarized in Table 3. As it is demonstrated in the table, the results indicated that the stability of functionalized-  $\text{Fe}_3\text{O}_4$  nanoparticles increased as nanoparticles concentration rose. Nevertheless, the  $\text{Fe}_3\text{O}_4$  nanoparticles had lower stability at higher concentration, demonstrating that the functionalization of iron oxide nanoparticles could enhance their stability.

#### 4.3. Impact of nanoparticles of on $\text{CO}_2$ absorption

Figs. 8–11 show the effect of bare and functionalized  $\text{Fe}_3\text{O}_4$  nanoparticles on  $\text{CO}_2$  loading at various concentrations, including 0.01, 0.03, and 0.05 wt%. Indeed, as a result, Fig. 12 illustrated that all nanofluids had higher  $\text{CO}_2$  absorption capabilities than the base fluid (10 wt% MDEA), and  $\text{CO}_2$  absorption was more positively influenced by amino acid functions.

As shown in Fig. 8, because magnetic nanoparticles were highly stable at 0.01 wt% than at higher concentrations,  $\text{Fe}_3\text{O}_4$  nanoparticles had a higher  $\text{CO}_2$  loading at lower concentrations. According to the results obtained,  $\text{Fe}_3\text{O}_4$  nanoparticles at 0.01 wt% concentration could increase  $\text{CO}_2$  loading by 0.65 mol  $\text{CO}_2$ /mole amine compared to 0.48 mol  $\text{CO}_2$ /mole amine for the base fluid. It is attributed to more effective mass transfer mechanism including shuttle effect, hydrodynamic effect and bubble breaking effect, due to nanoparticles greater stability. Also,  $\text{Fe}_3\text{O}_4$  nanofluids with 0.05 wt% had lower stability than the other  $\text{Fe}_3\text{O}_4$  nanofluids, and could increase  $\text{CO}_2$  loading only up to 0.497 mol  $\text{CO}_2$  per mole amine.

Furthermore, Fig. 8 shows the change in  $\text{CO}_2$  loading during the absorption process. This figure indicates that  $\text{CO}_2$  absorption was greater at the beginning and for the first 20 min. However, the  $\text{CO}_2$  loading of unstable  $\text{Fe}_3\text{O}_4$  nanofluids had a sharper trend than the stable  $\text{Fe}_3\text{O}_4$  nanofluids at the beginning (0–20 min). In other words,  $\text{Fe}_3\text{O}_4$  nanofluids with lower stability absorbed more  $\text{CO}_2$  molecules at first, but their ability to absorb  $\text{CO}_2$  decreased over time.

So, due to nanoparticles' increased tendency to agglomerate and sediment, they had a lower effective  $\text{CO}_2$  absorption at the end. However, the magnetic nanoparticles could still improve  $\text{CO}_2$  absorption in stable nanofluids, such as 0.01 wt%  $\text{Fe}_3\text{O}_4$  nanofluid, at the end of the absorption process (after 20 min).

Fig. 9 shows the  $\text{CO}_2$  loading of  $\text{Fe}_3\text{O}_4@\text{arg}$  nanofluids during the absorption process. As mentioned, the stability of nanofluids was considered a vital factor in promoting  $\text{CO}_2$  absorption mechanisms,

**Table 3**  
Absolute zeta potential measurements for different concentration of nanoparticles.

Nanofluid	Absolute zeta potential	Stability	Nanofluid	Absolute zeta potential	Stability
$\text{Fe}_3\text{O}_4$ (0.01 wt%)	44.5	Stable	$\text{Fe}_3\text{O}_4@\text{his}$ (0.01 wt%)	49.1	Stable
$\text{Fe}_3\text{O}_4$ (0.03 wt%)	43.2	Stable	$\text{Fe}_3\text{O}_4@\text{his}$ (0.03 wt%)	49.9	Stable
$\text{Fe}_3\text{O}_4$ (0.05 wt%)	40.9	Stable	$\text{Fe}_3\text{O}_4@\text{his}$ (0.05 wt%)	51.1	Stable
$\text{Fe}_3\text{O}_4@\text{arg}$ (0.01 wt%)	40	Stable	$\text{Fe}_3\text{O}_4@\text{gly}$ (0.01 wt%)	46.1	Stable
$\text{Fe}_3\text{O}_4@\text{arg}$ (0.03 wt%)	41.1	Stable	$\text{Fe}_3\text{O}_4@\text{gly}$ (0.03 wt%)	48.4	Stable
$\text{Fe}_3\text{O}_4@\text{arg}$ (0.05 wt%)	47.6	Stable	$\text{Fe}_3\text{O}_4@\text{gly}$ (0.05 wt%)	52.9	Stable

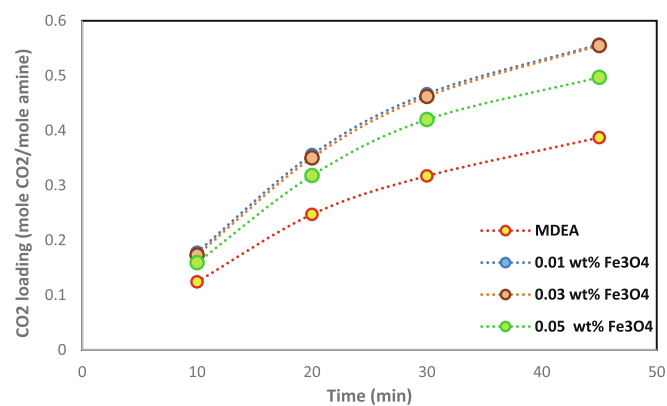


Fig. 8. Effect of bare  $\text{Fe}_3\text{O}_4$  nanoparticles concentration on  $\text{CO}_2$  loading during absorption experiments.

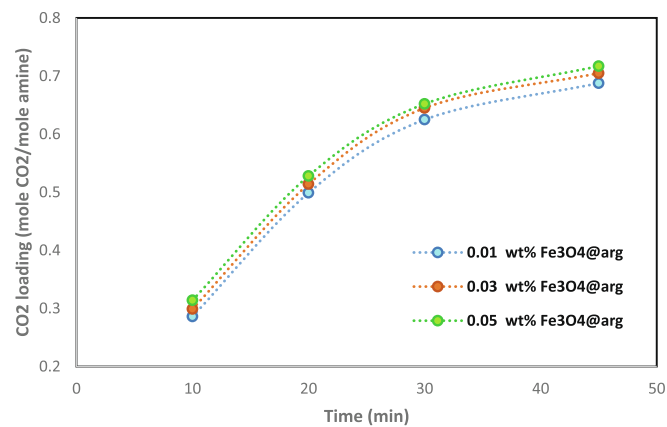


Fig. 9. Effect of  $\text{Fe}_3\text{O}_4@\text{arg}$  nanoparticles concentration on  $\text{CO}_2$  loading during absorption experiments.

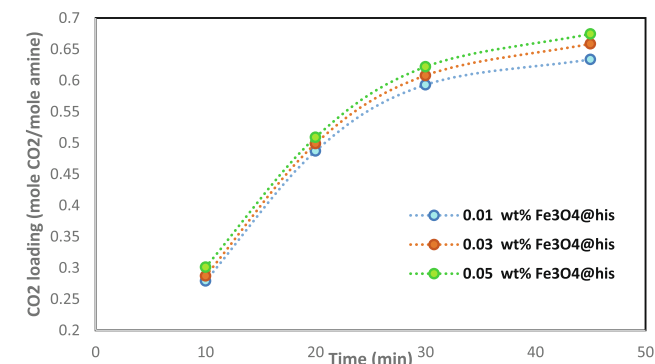
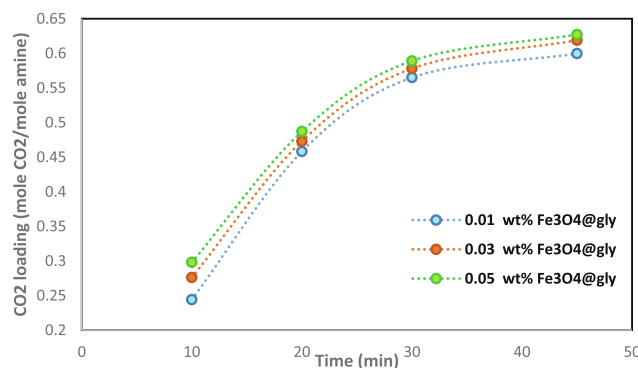


Fig. 10. Effect of  $\text{Fe}_3\text{O}_4@\text{his}$  nanoparticles concentration on  $\text{CO}_2$  loading during absorption experiments.

which could be investigated with the zeta potential analysis results. Based on the obtained results,  $\text{Fe}_3\text{O}_4@\text{arg}$  nanoparticles at 0.05 wt% concentration had a higher  $\text{CO}_2$  loading than the other concentrations because of their high absolute zeta potential and higher nanofluid stability.  $\text{CO}_2$  loading of  $\text{Fe}_3\text{O}_4@\text{arg}$  nanoparticles at concentrations of 0.01, 0.03, and 0.05 wt% was measured to be 0.779, 0.793, and 0.799, respectively.

The results demonstrate that functionalized nanoparticles with amino acids improved  $\text{CO}_2$  absorption through a variety of mechanisms. Indeed, the  $\text{CO}_2$  absorption performance of various  $\text{Fe}_3\text{O}_4@\text{his}$  nanofluids are demonstrated in Fig. 10. It is seen in this figure that  $\text{Fe}_3\text{O}_4@\text{his}$



**Fig. 11.** Effect of  $\text{Fe}_3\text{O}_4@\text{gly}$  nanoparticles concentration on  $\text{CO}_2$  loading during absorption experiments.

nanoparticles enhanced base fluid's ability to absorb  $\text{CO}_2$  by 0.776 at 0.05 wt% concentrations, which is likely due to higher nanofluid stability and more active particles compared to the other  $\text{Fe}_3\text{O}_4@\text{his}$  concentration.

Moreover, the  $\text{CO}_2$  loading versus time for  $\text{Fe}_3\text{O}_4@\text{gly}$  is shown in Fig. 11. As demonstrated, experimental results illustrated that  $\text{Fe}_3\text{O}_4@\text{gly}$  nanoparticles had a higher  $\text{CO}_2$  loading than bare  $\text{Fe}_3\text{O}_4$ , and its nanofluids could enhance  $\text{CO}_2$  loading by 0.718 at 0.05 wt% nanoparticles concentration, as optimum concentration.

Nevertheless, Fig. 12 compares the capabilities of different bare and functionalized  $\text{Fe}_3\text{O}_4$  nanofluids. Results of the experiments revealed that all nanofluids were more capable of enhancing  $\text{CO}_2$  absorption. Furthermore, Fig. 12 shows how the number of amine groups influences rising  $\text{CO}_2$  capture performance. By applying amino acids with more N-H groups at their chemical structure, more  $\text{CO}_2$  was captured due to intensified chemical and physical mechanisms. As a result, it was found that  $\text{Fe}_3\text{O}_4@\text{arg}$  improved  $\text{CO}_2$  absorption performance more than  $\text{Fe}_3\text{O}_4@\text{his}$  and  $\text{Fe}_3\text{O}_4@\text{gly}$  among functionalized magnetic nanoparticles.

In fact, magnetic nanoparticles could have increased  $\text{CO}_2$  absorption via some physical mechanisms, including Brownian motion, shuttle effect and hydrodynamic effect [68]. However, applying amino acids in nanoparticles could provide both the chemical and physical mechanisms for  $\text{CO}_2$  absorption due to the presence of N-H bonds in chemical structure of nanoparticles. Since amino acids could enhance the hydrophilic properties of magnetic nanoparticles, so functionalized nanoparticles had a greater impact on  $\text{CO}_2$  absorption than bare  $\text{Fe}_3\text{O}_4$  nanoparticles.

#### 4.4. Impact of bare $\text{Fe}_3\text{O}_4$ nanoparticles on $\text{CO}_2$ desorption

As seen in Fig. 13, the positive effect of various  $\text{Fe}_3\text{O}_4$  nanofluids on  $\text{CO}_2$  desorption was compared to base fluid. The obtained results demonstrated that all nanofluids had a significant effect on improving  $\text{CO}_2$  stripping. As it is evident in Fig. 13,  $\text{Fe}_3\text{O}_4$  at 0.03 wt% concentration increased  $\text{CO}_2$  volume fraction by 23.3% and 25.4% at 60 and 70 °C, respectively, at outlet gas stream. However, the regeneration efficiency decreased at higher concentrations of iron oxide nanoparticles. It was believed that several mechanisms which were involved in intensified  $\text{CO}_2$  desorption at nanoparticles caused this phenomenon. (See Fig. 14.).

As mentioned above, the hydrodynamic effects of nanoparticles at base fluid, such as bubble breaking mechanisms and micro-convection induced by Brownian motion, also had serious effects on improving  $\text{CO}_2$  desorption. Magnetic nanoparticles, however, had several thermal effects, including enhancing thermal conductivity and thermal diffusivity of base fluid. Therefore, it appeared that nanoparticles could improve  $\text{CO}_2$  desorption. Nonetheless, it was vital to investigate the stability of nanofluids. Based on the results of the zeta potential analysis,  $\text{Fe}_3\text{O}_4$  nanoparticles at higher concentrations of 0.01 wt% had a lower stability. Consequently, with higher nanoparticle concentrations, the hydrodynamic mechanism was limited by more agglomeration and sedimentation. On the other hand, thermal diffusivity of nanofluids was prompted by adding more metal oxide nanoparticles. Hence, due to acceptable stability and the number of available nanoparticles, 0.03 wt %  $\text{Fe}_3\text{O}_4$  nanoparticles was considered to be an optimum concentration, that had the highest  $\text{CO}_2$  desorption performance compared with the other  $\text{Fe}_3\text{O}_4$  nanofluids.

#### 4.5. Impact of functionalized- $\text{Fe}_3\text{O}_4$ nanoparticles on $\text{CO}_2$ desorption

In this study, a comparison was made between  $\text{CO}_2$  stripping in  $\text{Fe}_3\text{O}_4@\text{arg}$ ,  $\text{Fe}_3\text{O}_4@\text{his}$ , and  $\text{Fe}_3\text{O}_4@\text{gly}$  nanofluids at 60 and 70 °C regeneration temperatures and plain  $\text{Fe}_3\text{O}_4$  nanoparticles. Based on the experimental results, a higher  $\text{CO}_2$  desorption rate was observed for all functionalized nanoparticles than for bare  $\text{Fe}_3\text{O}_4$  nanofluids. Fig. 10 shows the results of  $\text{CO}_2$  stripping for bare  $\text{Fe}_3\text{O}_4$  and  $\text{Fe}_3\text{O}_4@\text{gly}$  nanoparticles based on concentrations of  $\text{Fe}_3\text{O}_4@\text{gly}$  nanoparticles in base fluid. As can be seen, the regeneration performance was increased by  $\text{Fe}_3\text{O}_4@\text{gly}$ , raising nanoparticles concentration. As a result of the Zeta potential analysis,  $\text{Fe}_3\text{O}_4@\text{gly}$  nanoparticles were found to be more stable at higher concentrations. However, the presence rather than the quantity of nanoparticles in the base fluid resulted in a higher average thermal conductivity of the nanofluid. Thus,  $\text{Fe}_3\text{O}_4@\text{gly}$  nanoparticles at 0.05 wt% were considered to be the best concentration for enhancing  $\text{CO}_2$  desorption, following 0.03 wt% and 0.01 wt%.

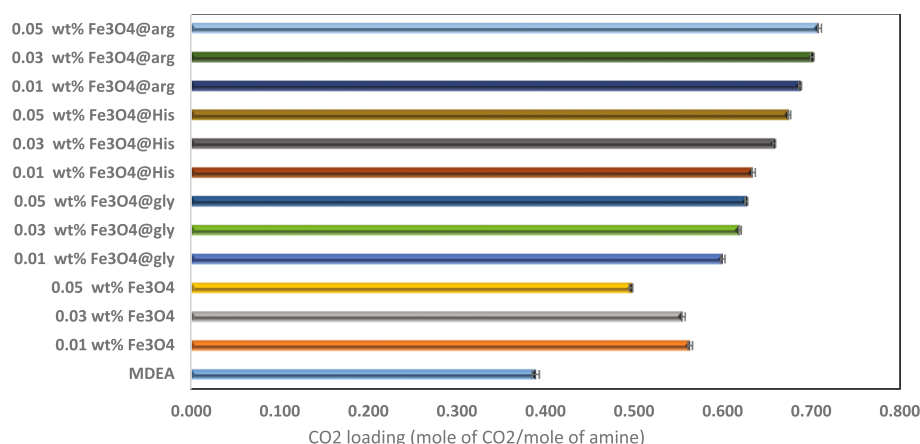


**Fig. 12.** Effect of nanoparticles type and concentration on  $\text{CO}_2$  loading at the end of absorption time.

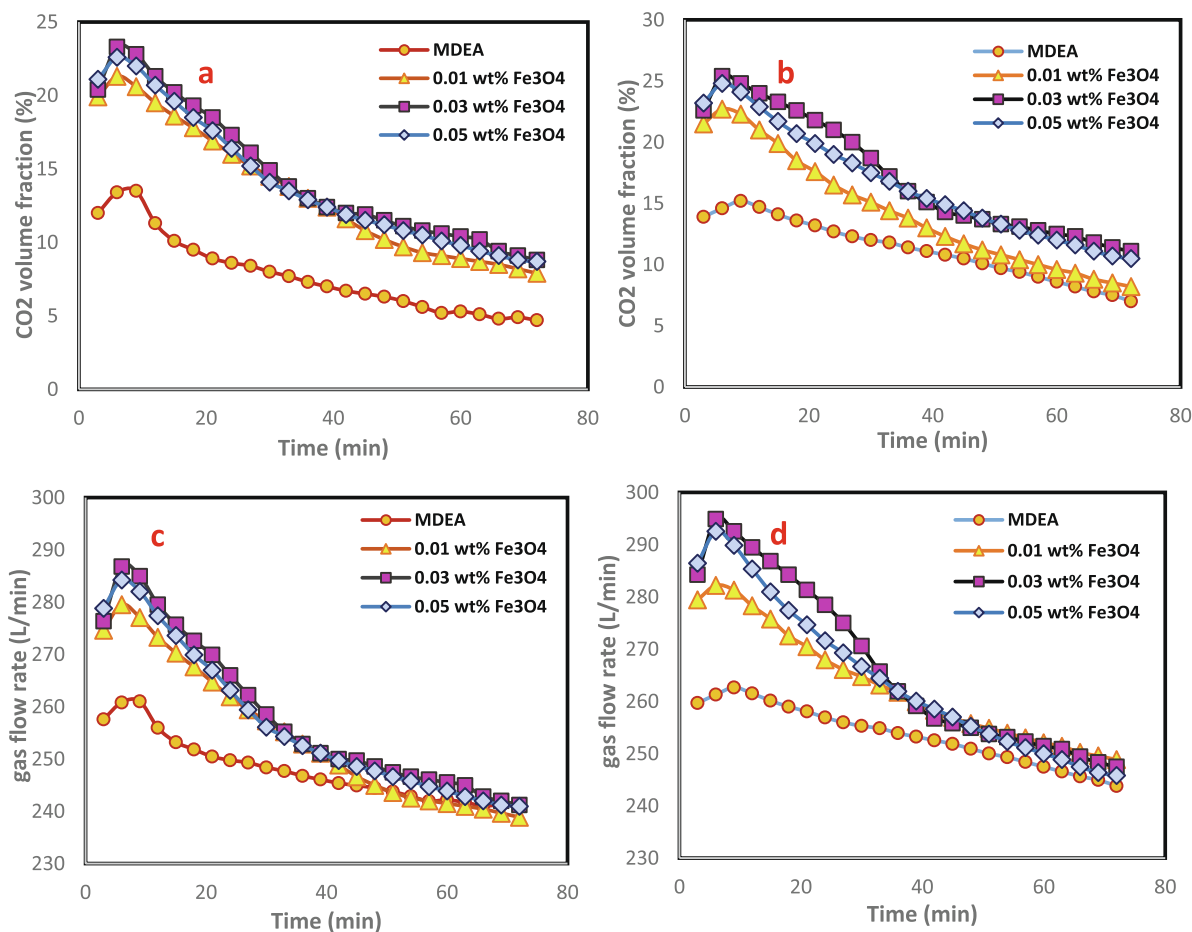


**Fig. 13.** Effect of Fe<sub>3</sub>O<sub>4</sub> nanofluids on CO<sub>2</sub> desorption during regeneration process with 200 mL/min purge air. **a)** Based on outlet CO<sub>2</sub> volume fraction at 60 °C; **b)** Based on outlet CO<sub>2</sub> volume fraction at 70 °C; **c)** Based on output gas flow rate at 60 °C; **d)** Based on output gas flow rate at 70 °C.

Consequently, the outlet gas flow rate and its CO<sub>2</sub> amount were 312 L/min and 0.35 (volume fraction) for 0.05 wt% Fe<sub>3</sub>O<sub>4</sub>@gly nanofluid at 70 °C, respectively, which were higher than those of plain Fe<sub>3</sub>O<sub>4</sub> nanofluids at best concentration. In fact, Fe<sub>3</sub>O<sub>4</sub>@gly was actually more stable than plain Fe<sub>3</sub>O<sub>4</sub>, which promoted heat and mass transfer mechanisms and resulted in more initial CO<sub>2</sub> loading and more CO<sub>2</sub> stripping.

Furthermore, as shown in Fig. 15, Fe<sub>3</sub>O<sub>4</sub>@his nanoparticle also improved CO<sub>2</sub> stripping. What's more, compared to bare Fe<sub>3</sub>O<sub>4</sub> nanoparticles the functionalized iron oxide nanoparticles were more stable. Therefore, it was expected that in the presence of nanoparticles, functionalized Fe<sub>3</sub>O<sub>4</sub> could be more efficient in intensifying mass and heat transfer mechanisms.

Similarly, Fe<sub>3</sub>O<sub>4</sub>@his nanofluids behaved exactly like the Fe<sub>3</sub>O<sub>4</sub>@gly nanofluids. In the presence of Fe<sub>3</sub>O<sub>4</sub>@his nanoparticles, the best CO<sub>2</sub> desorption performance was therefore achieved at 0.05 wt%, which was considered an optimum concentration.

Fig. 16 shows the same results for Fe<sub>3</sub>O<sub>4</sub>@arg nanofluids. According to the obtained results, Fe<sub>3</sub>O<sub>4</sub>@arg nanoparticles behaved like other functionalized nanoparticles. The Fe<sub>3</sub>O<sub>4</sub>@arg nanoparticles at 0.05 wt% concentration were found to have a higher capacity in enhancing CO<sub>2</sub> desorption than those at the lower concentrations, which was explained by high stability and greater initial CO<sub>2</sub> loading. Hence, more CO<sub>2</sub> absorption by physical and chemical mechanisms led to higher regeneration efficiency.

In Fig. 17, the CO<sub>2</sub> desorption performance of plain Fe<sub>3</sub>O<sub>4</sub> and functionalized Fe<sub>3</sub>O<sub>4</sub> nanofluids was compared at 70 °C regeneration temperature at optimal concentrations. As depicted in Fig. 17, following

Fe<sub>3</sub>O<sub>4</sub>@arg, Fe<sub>3</sub>O<sub>4</sub>@his and Fe<sub>3</sub>O<sub>4</sub>@gly nanoparticles had a higher outlet gas flow rate and a higher CO<sub>2</sub> volume fraction than bare Fe<sub>3</sub>O<sub>4</sub> at optimal concentrations. This is related to chemical reaction between CO<sub>2</sub> molecules and amino groups embedded into their chemical structure. On the other hand, the results of the zeta potential analysis demonstrated that the presence of amino groups in iron oxide nanoparticles' structure led to more stability of nanofluids by modified magnetic nanoparticles. Consequently, functionalized Fe<sub>3</sub>O<sub>4</sub> could be more efficient in improving mass and heat transfer mechanisms at higher concentrations and they had a more positive effect in enhancing CO<sub>2</sub> desorption from 10 wt% MDEA solution than the bare Fe<sub>3</sub>O<sub>4</sub> nanoparticles.

Furthermore, to facilitate a better comparison, Fig. 18 displayed the experimental results of CO<sub>2</sub> loading at the end of CO<sub>2</sub> absorption and desorption tests. Accordingly, the final CO<sub>2</sub> loading at the end of desorption time and the CO<sub>2</sub> loading difference between absorption and desorption tests were considered two essential factors to compare the CO<sub>2</sub> stripping performance of nanofluids. As it was shown, for all nanofluids, the CO<sub>2</sub> loading at the end of the regeneration process had a lower value at 70 °C than the 60 °C regeneration temperature, which indicates more CO<sub>2</sub> was released from the nanofluids at 70 °C. On the other hand, the CO<sub>2</sub> loading had a higher falling rate for functionalized Fe<sub>3</sub>O<sub>4</sub> nanoparticles than the bare Fe<sub>3</sub>O<sub>4</sub>. Hence, the results clearly depicted that modified magnetic nanoparticles were capable of improving CO<sub>2</sub> absorption and nanofluid regeneration.

Fig. 18 shows the CO<sub>2</sub> loading was decreased by 29.6%, 40.4% and 39.5% when Fe<sub>3</sub>O<sub>4</sub> nanofluids were 0.01, 0.03, and 0.05 wt% at 70 °C, respectively, which was consistent with the gas phase analysis results

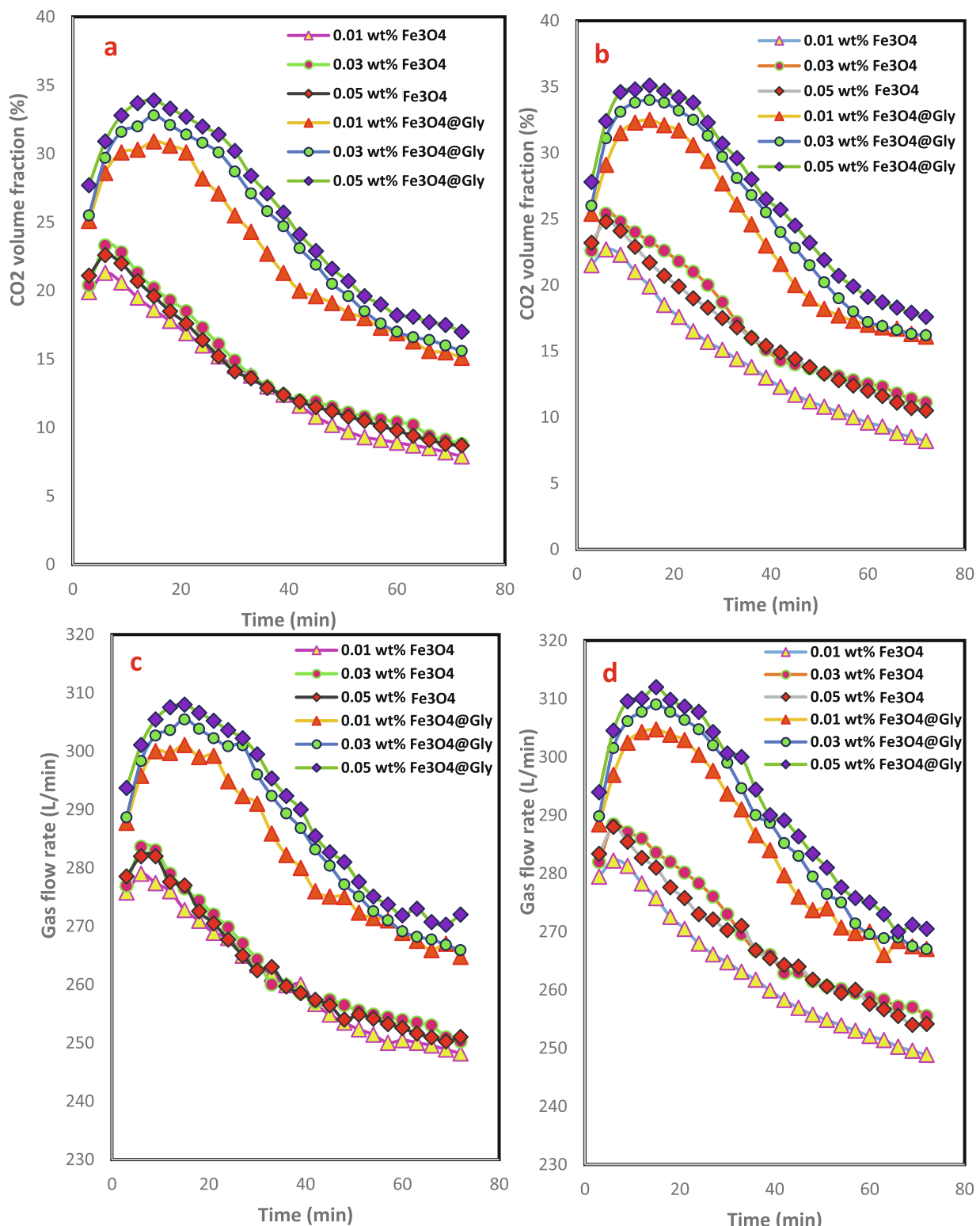


**Fig. 14.** Effect of  $\text{Fe}_3\text{O}_4$ @gly nanofluids on  $\text{CO}_2$  desorption during regeneration process with  $200 \text{ mL/min}$  purge air. **a)** Based on outlet  $\text{CO}_2$  volume fraction at  $60^\circ\text{C}$ ; **b)** Based on outlet  $\text{CO}_2$  volume fraction at  $70^\circ\text{C}$ ; **c)** Based on output gas flow rate at  $60^\circ\text{C}$ ; **d)** Based on output gas flow rate at  $70^\circ\text{C}$ .

(outlet gas flow rate and  $\text{CO}_2$  volume fraction). Consequently,  $\text{Fe}_3\text{O}_4$  nanoparticles showed higher capability in improving  $\text{CO}_2$  stripping performance at 0.03 wt% concentration because  $\text{CO}_2$  loading decreased more rapidly. However, functionalized magnetic nanoparticles showed a different trend. As mentioned before, by applying amino acids to its surface,  $\text{Fe}_3\text{O}_4$  nanoparticles were more stable at the base fluid. Thus,

functionalized  $\text{Fe}_3\text{O}_4$  nanoparticles increased  $\text{CO}_2$  desorption performance at higher concentrations, as indicated by gas phase analysis. The reported results in Fig. 18 demonstrates this trend. Obtained results indicated that  $\text{CO}_2$  loading decreased by 36.2%, 44.6% and 46.1% at 0.01, 0.03 and 0.05 wt%  $\text{Fe}_3\text{O}_4@\text{gly}$  concentrations at  $70^\circ\text{C}$  regeneration temperature, respectively. Furthermore, at  $70^\circ\text{C}$  the falling rate of

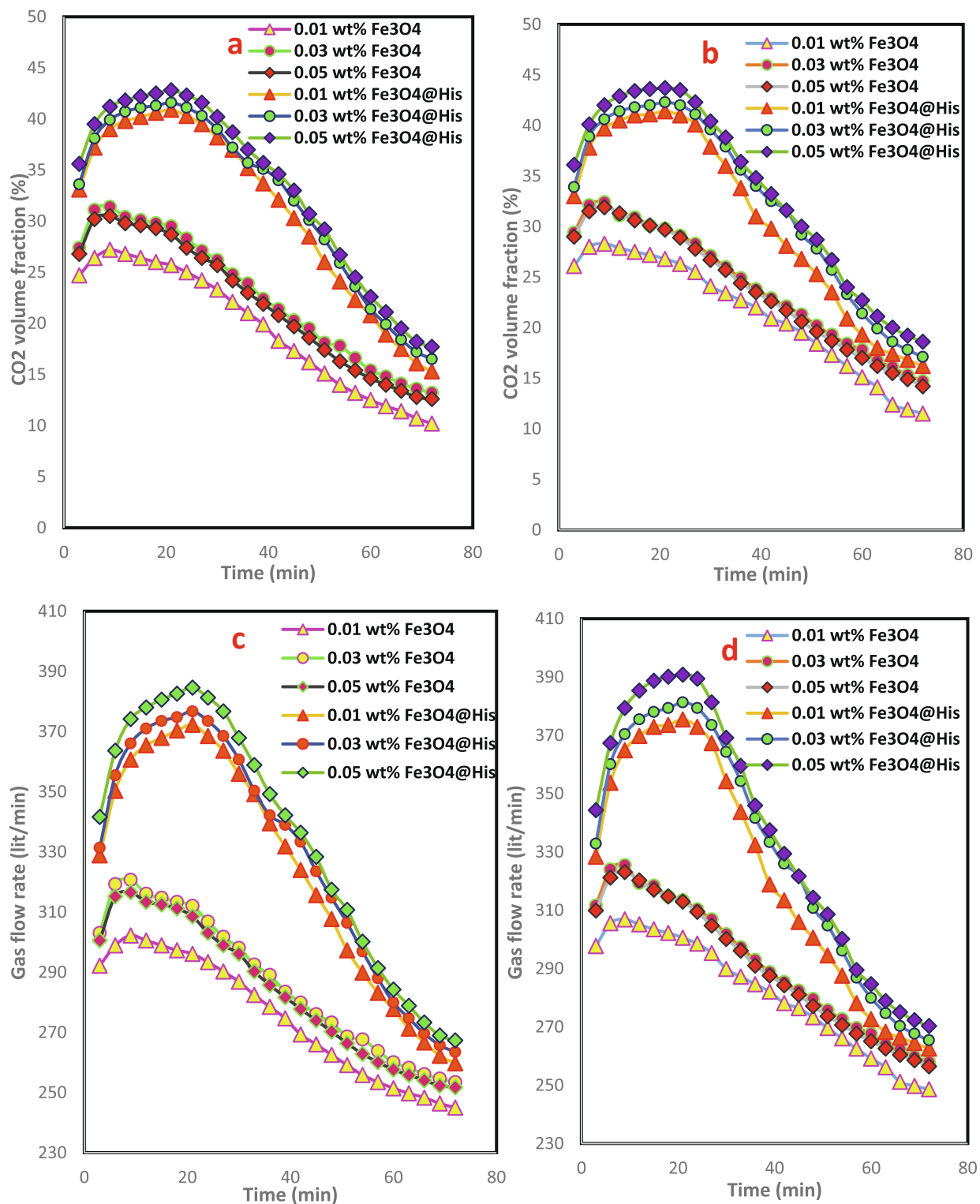


**Fig. 15.** Effect of  $\text{Fe}_3\text{O}_4@\text{His}$  nanofluids on  $\text{CO}_2$  desorption during regeneration process with 200 mL/min purge air. **a)** Based on outlet  $\text{CO}_2$  volume fraction at 60 °C; **b)** Based on outlet  $\text{CO}_2$  volume fraction at 70 °C; **c)** Based on output gas flow rate at 60 °C; **d)** Based on output gas flow rate at 70 °C.

$\text{CO}_2$  loading was 38.7%, 45.7% and 47.2% at  $\text{Fe}_3\text{O}_4@\text{His}$  concentrations of 0.01, 0.03, and 0.05 wt%.

In contrast, more N–H groups in the chemical structure of  $\text{Fe}_3\text{O}_4@\text{arg}$  nanoparticles resulted in more efficient nanofluids. As it is evident in this figure, with concentrations of 0.01, 0.03 and 0.05 wt%,  $\text{Fe}_3\text{O}_4@\text{arg}$  nanoparticles can reduce  $\text{CO}_2$  loading by 39.8%, 46.4% and 48.2% at the end of the desorption process at 70 °C. Therefore, Fig. 18 clearly shows

that all bare and functionalized  $\text{Fe}_3\text{O}_4$  nanoparticles reduce energy consumption during regeneration process because more  $\text{CO}_2$  desorption occurs at low temperatures.

## 5. Conclusions

The purpose of this study was to investigate the effectiveness of three

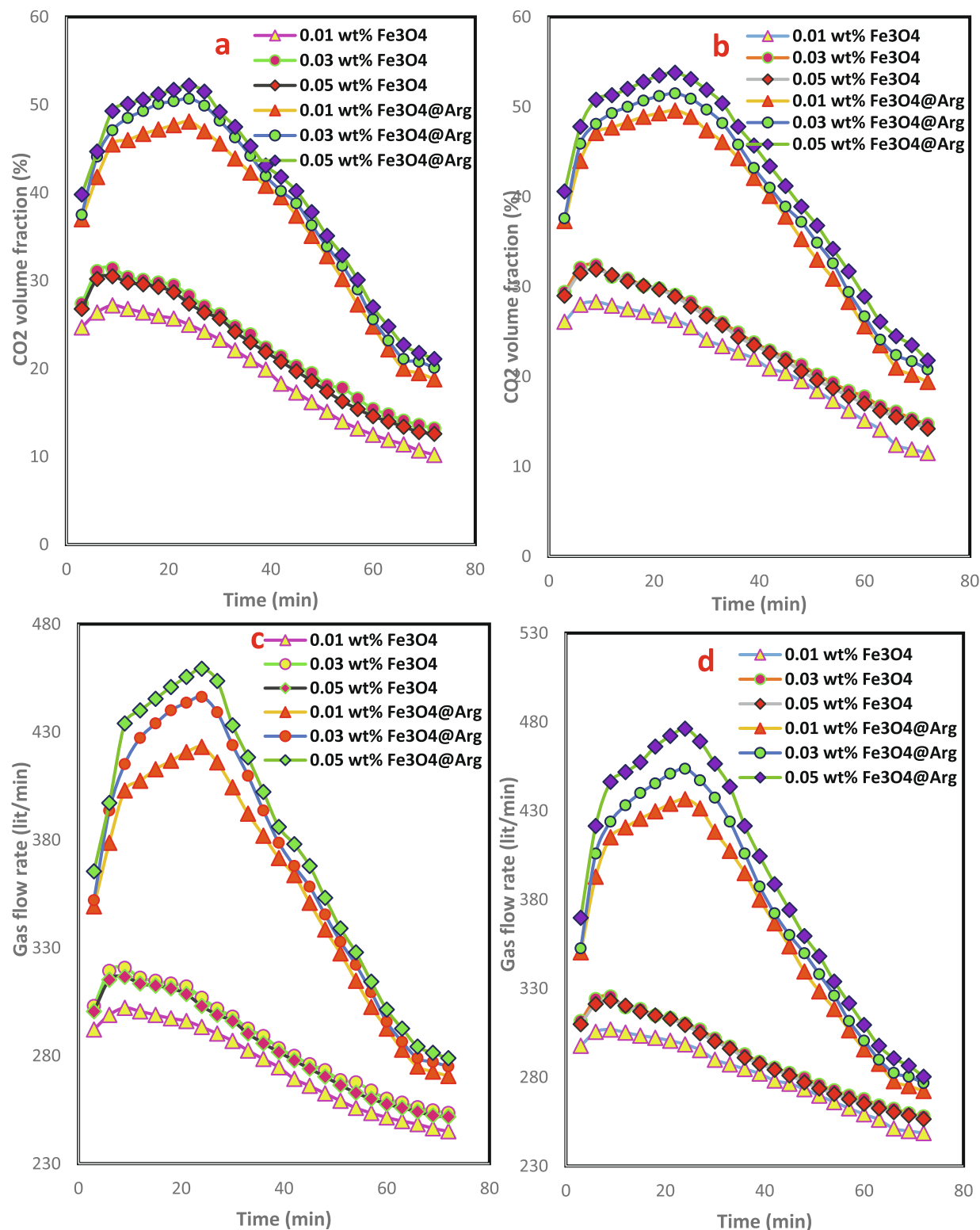


**Fig. 16.** Effect of  $\text{Fe}_3\text{O}_4$ @arg nanofluids on  $\text{CO}_2$  desorption during regeneration process with  $200 \text{ mL/min}$  purge air. **a)** Based on outlet  $\text{CO}_2$  volume fraction at  $60^\circ\text{C}$ ; **b)** Based on outlet  $\text{CO}_2$  volume fraction at  $70^\circ\text{C}$ ; **c)** Based on output gas flow rate at  $60^\circ\text{C}$ ; **d)** Based on output gas flow rate at  $70^\circ\text{C}$ .

different functionalized  $\text{Fe}_3\text{O}_4$  nanoparticles in improving  $\text{CO}_2$  absorption and desorption. To do this, the arginine, histidine, and glycine amino acids were applied to the surface of  $\text{Fe}_3\text{O}_4$  nanoparticles. Indeed, all experimental tests were conducted with a semi-batch bubble column at ambient pressure. At  $20^\circ\text{C}$ , the experimental results of  $\text{CO}_2$  absorption were measured as  $\text{CO}_2$  loading in nanofluid. According to the

results, the functionalized nanoparticles were more stable in base fluid due to the presence of hydrophilic agents (amine groups) in their chemical structure. Thus, modified iron oxide nanoparticles were more capable of improving  $\text{CO}_2$  absorption due to their high stability and either physical or chemical mechanism for  $\text{CO}_2$  absorption. Since  $\text{Fe}_3\text{O}_4$ @arg had more amine groups than the other functionalized iron

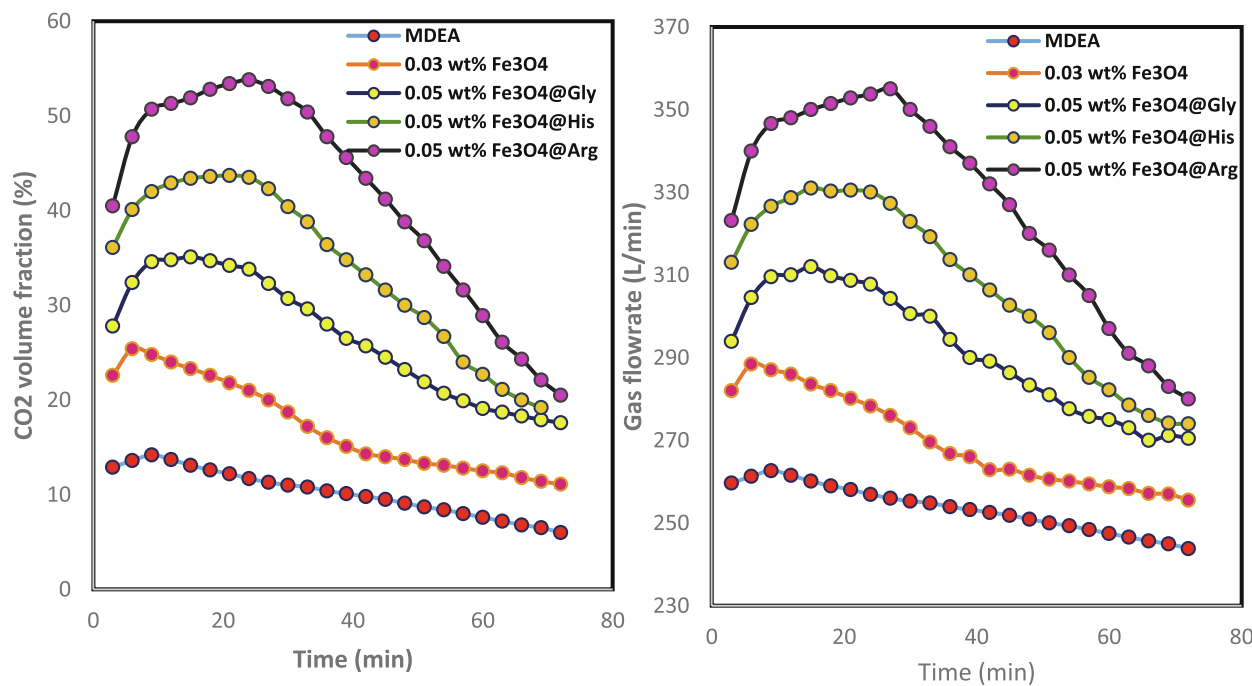


**Fig. 17.** Effect of different functionalized and bare Fe<sub>3</sub>O<sub>4</sub> nanoparticles at optimum concentrations on CO<sub>2</sub> desorption at 70 °C regeneration temperature and 200 mL/min purge air. **a)** Based on outlet CO<sub>2</sub> volume fraction; **b)** Based on output gas flow rate.

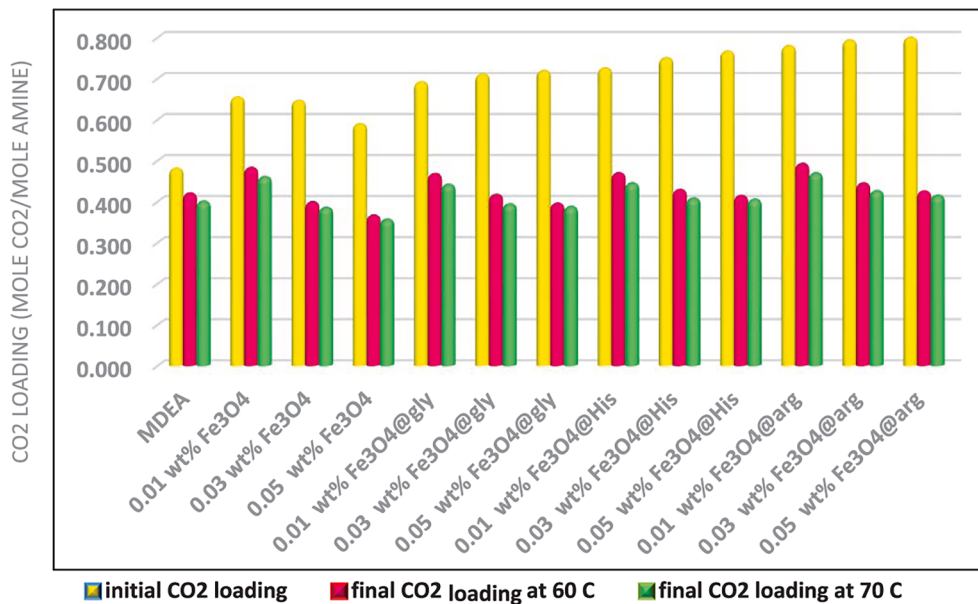


**Fig. 18.** Effect of different nanofluids on the final CO<sub>2</sub> loading at the end of 72 min regeneration process with different temperature.

oxide nanoparticles, it caused more chemical reaction between amines and CO<sub>2</sub> molecules, which is why it performed better at 0.05 wt% concentration. In contrast, at atmospheric pressure, Fe<sub>3</sub>O<sub>4</sub>@arg, Fe<sub>3</sub>O<sub>4</sub>@his, and Fe<sub>3</sub>O<sub>4</sub>@gly at 0.05 wt% concentration increased CO<sub>2</sub> absorption by 23%, 17%, and 10%, respectively, compared to bare Fe<sub>3</sub>O<sub>4</sub>. In addition, the regeneration experiments were conducted at 60 and 70 °C. Finally, the results indicated that functionalized Fe<sub>3</sub>O<sub>4</sub> nanoparticles improved CO<sub>2</sub> desorption performance by increasing initial loading and influencing hydrodynamics to a greater extent. Therefore, with Fe<sub>3</sub>O<sub>4</sub>@arg, Fe<sub>3</sub>O<sub>4</sub>@his, and Fe<sub>3</sub>O<sub>4</sub>@gly at the best concentration, decreased CO<sub>2</sub> loading by 48.2%, 47.2%, and 46.1% at 70 °C regeneration temperature, respectively. Finally, it deduced that,

although modified Fe<sub>3</sub>O<sub>4</sub> nanoparticles had a serious effect on promoting CO<sub>2</sub> absorption, they could increase CO<sub>2</sub> desorption's efficiency to a great extent.

#### Author information

Ethical Approval: Not applicable.

Consent to Participate: Not applicable.

Consent to Publish: Not applicable.

Corresponding Author.

Peyman Keshavarz.

#### Funding Sources

This work was financially supported by Shiraz University, Shiraz, Iran (No. 7134851154).

## CRediT authorship contribution statement

**Fariba Zarei:** Methodology, Data curation, Investigation, Resources, Writing – review & editing. **Peyman Keshavarz:** Conceptualization, Visualization, Supervision, Project administration, Funding acquisition.

## Declaration of Competing Interest

The authors declare that they have no known competing financial interests or personal relationships that could have appeared to influence the work reported in this paper.

## Data availability

Data will be made available on request.

## Acknowledgment

The authors would like to thank Shiraz University for supporting this research.

## References

- [1] J.W. Lee, et al., Combined CO<sub>2</sub> absorption/regeneration performance enhancement by using nanoabsorbents. 178 (2016) 164–176.
- [2] J. Jiang, et al., Experimental study of CO<sub>2</sub> absorption in aqueous MEA and MDEA solutions enhanced by nanoparticles. 29 (2014) 135–141.
- [3] Q. Zhou, et al., A comparative of life cycle assessment of post-combustion, pre-combustion and oxy-fuel CO<sub>2</sub> capture, Energy Procedia 63 (2014) 7452–7458.
- [4] C. Kunze, H. Spleithoff, Assessment of oxy-fuel, pre-and post-combustion-based carbon capture for future IGCC plants, Applied Energy 94 (2012) 109–116.
- [5] F. Zarei, et al., Insight into the experimental and modeling study of process intensification for post-combustion CO<sub>2</sub> capture by rotating packed bed, Journal of cleaner production 211 (2019) 953–961.
- [6] M. Kanniche, et al., Pre-combustion, post-combustion and oxy-combustion in thermal power plant for CO<sub>2</sub> capture, Applied Thermal Engineering 30 (1) (2010) 53–62.
- [7] R. Notz, et al., Selection and pilot plant tests of new absorbents for post-combustion carbon dioxide capture, Chemical Engineering Research and Design 85 (4) (2007) 510–515.
- [8] A.M. Yousef, et al., Upgrading biogas by a low-temperature CO<sub>2</sub> removal technique, Alexandria Engineering Journal 55 (2) (2016) 1143–1150.
- [9] S.D. Barnicki, J.R. Fair, Separation system synthesis: A knowledge-based approach. 2. Gas/vapor mixtures, Industrial & engineering chemistry research 31 (7) (1992) 1679–1694.
- [10] A. Ortiz, et al., Room temperature ionic liquid with silver salt as efficient reaction media for propylene/propane separation: Absorption equilibrium, Separation and Purification Technology 63 (2) (2008) 311–318.
- [11] M. Bohloul, A. Vatani, S.J.F.P.E. Peyghambarzadeh, Experimental and theoretical study of CO<sub>2</sub> solubility in N-methyl-2-pyrrolidone (NMP). 365 (2014) 106–111.
- [12] D. Wei, et al., An experimental and theoretical study on the effects of amine chain length on CO<sub>2</sub> absorption performance, AIChE Journal 69 (4) (2023) e17960.
- [13] P.C. Sahoo, et al., Biocatalyzed accelerated post-combustion CO<sub>2</sub> capture and stripping in monoethanolamine, Energy & Fuels 31 (10) (2017) 11007–11012.
- [14] W. Srisang, et al., CO<sub>2</sub> capture efficiency and heat duty of solid acid catalyst-aided CO<sub>2</sub> desorption using blends of primary-tertiary amines, International Journal of Greenhouse Gas Control 69 (2018) 52–59.
- [15] Z. Liang, et al., Experimental study on the solvent regeneration of a CO<sub>2</sub>-loaded MEA solution using single and hybrid solid acid catalysts, AIChE Journal 62 (3) (2016) 753–765.
- [16] P.A. Osei, et al., Mass transfer studies on catalyst-aided CO<sub>2</sub> desorption from CO<sub>2</sub>-loaded amine solution in a post-combustion CO<sub>2</sub> capture plant, Chemical Engineering Science 170 (2017) 508–517.
- [17] X. Zhang, et al., Reducing energy consumption of CO<sub>2</sub> desorption in CO<sub>2</sub>-loaded aqueous amine solution using Al<sub>2</sub>O<sub>3</sub>/HZSM-5 bifunctional catalysts, Applied Energy 229 (2018) 562–576.
- [18] X. Zhang, et al., Reduction of energy requirement of CO<sub>2</sub> desorption from a rich CO<sub>2</sub>-loaded MEA solution by using solid acid catalysts, Applied Energy 202 (2017) 673–684.
- [19] S. Gantert, D. Möller, Ultrasonic desorption of CO<sub>2</sub>—a new technology to save energy and prevent solvent degradation, Chemical engineering & technology 35 (3) (2012) 576–578.
- [20] H. Liu, et al., Ultrasonic enhancement of CO<sub>2</sub> desorption from MDEA solution in microchannels, Industrial & Engineering Chemistry Research 58 (4) (2019) 1711–1719.
- [21] J. Ying, et al., Ultrasound intensified CO<sub>2</sub> desorption from pressurized loaded monoethanolamine solutions, I. parameters investigation and modelling. Energy 163 (2018) 168–179.
- [22] J. Ying, et al., Ultrasound intensify CO<sub>2</sub> desorption from pressurized loaded monoethanolamine solutions, II. Optimization and cost estimation. Energy 173 (2019) 218–228.
- [23] O.Y. Orhan, et al., Ultrasound-assisted desorption of CO<sub>2</sub> from carbon dioxide binding organic liquids, Energy Procedia 114 (2017) 66–71.
- [24] S. Tsubaki, et al., Insights into the dielectric-heating-enhanced regeneration of CO<sub>2</sub>-rich aqueous amine solutions, ACS Sustainable Chemistry & Engineering 8 (36) (2020) 13593–13599.
- [25] J. Yang, et al., CO<sub>2</sub> capture by dry alkanolamines and an efficient microwave regeneration process, Journal of Materials Chemistry A 3 (12) (2015) 6440–6446.
- [26] T. Chronopoulos, et al., CO<sub>2</sub> desorption via microwave heating for post-combustion carbon capture, Microporous and mesoporous materials 197 (2014) 288–290.
- [27] F. Bougie, X. Fan, Microwave regeneration of monoethanolamine aqueous solutions used for CO<sub>2</sub> capture, International Journal of Greenhouse Gas Control 79 (2018) 165–172.
- [28] S.J. McGurk, et al., Microwave swing regeneration of aqueous monoethanolamine for post-combustion CO<sub>2</sub> capture, Applied energy 192 (2017) 126–133.
- [29] G. Durán-Jiménez, et al., Rapid, simple and sustainable synthesis of ultra-microporous carbons with high performance for CO<sub>2</sub> uptake, via microwave heating, Chemical Engineering Journal 388 (2020) 124309.
- [30] W. Zheng, et al., New method of kinetic modeling for CO<sub>2</sub> absorption into blended amine systems: A case of MEA/EAE/3DEA1P trisolvent blends, AIChE Journal 68 (6) (2022) e17628.
- [31] S.Z. Bolourchian Tabrizi, S. Shahhosseini, A. Ghaemi, Insights into the mass transfer mechanisms of nanofluids: A CO<sub>2</sub> absorption study, Energy & Fuels 35 (24) (2021) 20172–20184.
- [32] A. Elhambakhsh, et al., Synthesis of different modified magnetic nanoparticles for selective physical/chemical absorption of CO<sub>2</sub> in a bubble column reactor, Journal of Environmental Chemical Engineering 8 (5) (2020) 104195.
- [33] Choi, S.U. and J.A. Eastman, *Enhancing thermal conductivity of fluids with nanoparticles*. 1995, Argonne National Lab.(ANL), Argonne, IL (United States).
- [34] P. Kebinski, et al., Mechanisms of heat flow in suspensions of nano-sized particles (nanofluids), International journal of heat and mass transfer 45 (4) (2002) 855–863.
- [35] Prasher, R., P. Bhattacharya, and P.E. Phelan, *Brownian-motion-based convective-conductive model for the effective thermal conductivity of nanofluids*. 2006.
- [36] J.S. Lee, J.W. Lee, Y.T. Kang, CO<sub>2</sub> absorption/regeneration enhancement in DI water with suspended nanoparticles for energy conversion application, Applied energy 143 (2015) 119–129.
- [37] W. Yu, et al., CO<sub>2</sub> absorption/desorption enhanced by nanoparticles in post-combustion CO<sub>2</sub> capture. International Symposium on Coal Combustion, Springer, 2015.
- [38] J.W. Lee, et al., Combined CO<sub>2</sub> absorption/regeneration performance enhancement by using nanoabsorbents, Applied energy 178 (2016) 164–176.
- [39] T. Wang, et al., Enhanced CO<sub>2</sub> absorption and desorption by monoethanolamine (MEA)-based nanoparticle suspensions, Industrial & Engineering Chemistry Research 55 (28) (2016) 7830–7838.
- [40] Shakir, S.W., S.M.R. Ahmed, and A.D. Wiheeb, *Improvement of CO<sub>2</sub> Absorption/Desorption Rate Using New Nano-Fluid*. J, 2021, 39(3): p. 851–857.
- [41] A. Hafizi, M. Rajabzadeh, R. Khalifeh, Enhanced CO<sub>2</sub> absorption and desorption efficiency using DETA functionalized nanomagnetite/water nano-fluid, Journal of Environmental Chemical Engineering 8 (4) (2020) 103845.
- [42] F. Zarei, P. Keshavarz, Intensification of CO<sub>2</sub> absorption and desorption by metal/non-metal oxide nanoparticles in bubble columns, Environmental Science and Pollution Research (2022) 1–14.
- [43] Y. Li, et al., CO<sub>2</sub> absorption and desorption enhancement by nano-SiO<sub>2</sub> in DBU-glycerol solution with high viscosity, Separation and Purification Technology 309 (2023) 122983.
- [44] A. Akbarzadeh, M. Samiei, S. Davaran, Magnetic nanoparticles: preparation, physical properties, and applications in biomedicine, Nanoscale research letters 7 (1) (2012) 1–13.
- [45] F. Zarei, et al., Enhanced CO<sub>2</sub> absorption and reduced regeneration energy consumption using modified magnetic NPs, Energy (2023) 127776.
- [46] K.R. Chaturvedi, R. Narukulla, T. Sharma, CO<sub>2</sub> capturing evaluation of single-step silica nanofluid through rheological investigation for nanofluid use in carbon utilization applications, Journal of Molecular Liquids 304 (2020) 112765.
- [47] Z. Zhang, et al., Progress in enhancement of CO<sub>2</sub> absorption by nanofluids: A mini review of mechanisms and current status, Renewable energy 118 (2018) 527–535.
- [48] H. Rashidi, S. Manivand, Experimental and numerical mass transfer study of carbon dioxide absorption using Al<sub>2</sub>O<sub>3</sub>/water nanofluid in wetted wall column, Energy 238 (2022) 121670.
- [49] Santos, S.P.d., *Comparative study of amine solutions used in CO<sub>2</sub> absorption/desorption cycles*. 2013, Instituto Superior de Engenharia de Lisboa.
- [50] C. Pang, J.W. Lee, Y.T. Kang, Review on combined heat and mass transfer characteristics in nanofluids, International Journal of Thermal Sciences 87 (2015) 49–67.
- [51] M. Khan, A revised model to analyze the heat and mass transfer mechanisms in the flow of carreau nanofluids, International Journal of Heat and Mass Transfer 103 (2016) 291–297.
- [52] B.M. Tehrani, A. Rahbar-Kelishami, Influence of enhanced mass transfer induced by brownian motion on supported nanoliquids membrane: Experimental correlation and numerical modelling, International Journal of Heat and Mass Transfer 148 (2020) 119034.
- [53] W.-G. Kim, et al., Synthesis of silica nanofluid and application to CO<sub>2</sub> absorption, Separation Science and Technology 43 (11–12) (2008) 3036–3055.

- [54] S.-Y. Cheng, Y.-Z. Liu, G.-S. Qi, Progress in the enhancement of gas–liquid mass transfer by porous nanoparticle nanofluids, *Journal of Materials Science* 54 (20) (2019) 13029–13044.
- [55] H. Pashaei, A. Ghaemi, CO<sub>2</sub> absorption into aqueous diethanolamine solution with nano heavy metal oxide particles using stirrer bubble column: Hydrodynamics and mass transfer, *Journal of Environmental Chemical Engineering* 8 (5) (2020) 104110.
- [56] X. Feng, D.W. Johnson, Mass transfer in SiO<sub>2</sub> nanofluids: A case against purported nanoparticle convection effects, *International Journal of Heat and Mass Transfer* 55 (13–14) (2012) 3447–3453.
- [57] X. Fang, Y. Xuan, Q. Li, Experimental investigation on enhanced mass transfer in nanofluids, *Applied Physics Letters* 95 (20) (2009) 203108.
- [58] L. Li, Y.T. Kang, Enhancement mechanisms of mass transfer performance by nanoabsorbents during CO<sub>2</sub> absorption process, *International Journal of Heat and Mass Transfer* 164 (2021) 120444.
- [59] J.H. Kim, C.W. Jung, Y.T. Kang, Mass transfer enhancement during CO<sub>2</sub> absorption process in methanol/Al2O<sub>3</sub> nanofluids, *International journal of heat and mass transfer* 76 (2014) 484–491.
- [60] A. Ghadimi, R. Saidur, H. Metselaar, A review of nanofluid stability properties and characterization in stationary conditions, *International journal of heat and mass transfer* 54 (17–18) (2011) 4051–4068.
- [61] G. Nematbakhsh, A. Rahbar-Kelishami, The effect of size and concentration of nanoparticles on the mass transfer coefficients in irregular packed liquid–liquid extraction columns, *Chemical Engineering Communications* 202 (11) (2015) 1493–1501.
- [62] A. Zaraki, et al., Theoretical analysis of natural convection boundary layer heat and mass transfer of nanofluids: Effects of size, shape and type of nanoparticles, type of base fluid and working temperature, *Advanced Powder Technology* 26 (3) (2015) 935–946.
- [63] J. Fan, L. Wang, Review of heat conduction in nanofluids, *Journal of heat transfer* 133 (4) (2011).
- [64] S. Bhattacharjee, DLS and zeta potential—what they are and what they are not? *Journal of controlled release* 235 (2016) 337–351.
- [65] A. Sankhla, et al., Biosynthesis and characterization of cadmium sulfide nanoparticles—an emphasis of zeta potential behavior due to capping, *Materials Chemistry and Physics* 170 (2016) 44–51.
- [66] C.O. Metin, et al., Stability of aqueous silica nanoparticle dispersions, *Journal of Nanoparticle Research* 13 (2) (2011) 839–850.
- [67] N. Sizachenko, et al., Zeta potentials ( $\zeta$ ) of metal oxide nanoparticles: A meta-analysis of experimental data and a predictive neural networks modeling, *NanoImpact* 22 (2021) 100317.
- [68] B. Rahmatmand, P. Keshavarz, S. Ayatollahi, Study of absorption enhancement of CO<sub>2</sub> by SiO<sub>2</sub>, Al2O<sub>3</sub>, CNT, and Fe3O<sub>4</sub> nanoparticles in water and amine solutions, *Journal of Chemical & Engineering Data* 61 (4) (2016) 1378–1387.